Microfluid Nanofluid (2014) 17:477–488
DOI 10.1007/s10404-014-1331-0

RESEARCH PAPER

A bead-based single nucleotide polymorphism (SNP) detection using melting temperature on a microchip

Pei-Chun Kao · Shih-Torng Ding · En-Chung Lin · Kan-Chien Li · Lon Wang · Yen-Wen Lu

Received: 15 July 2013 / Accepted: 4 January 2014 / Published online: 10 January 2014

Abstract Single nucleotide polymorphism (SNP) is not only one of the most common genetic variances in a human genome, but it also serves a crucial biomarker greatly affecting the phenotypes of individuals. Moreover, SNP had shown its importance by making contributions in many aspects, including species classification for pests, pesticide resistance detection, and disease diagnostic for human beings. Most of today's SNP detection techniques utilize enzymes or modification of DNA, leading to the requirement of high reagent cost or complex procedures. Therefore, a new SNP genotyping scheme has been developed to address these issues by conducting melting curve analysis on the DNA target sequences, which are conjugated onto polystyrene microbeads in a microfluidic device. The microbeads function as a solid vehicle for capturing the DNA duplexes, providing a larger surface-to-volume ratio for reaction and allowing it to be hydrodynamically confined for melting curve analysis. A prototype device serving as a basis for this proposed scheme was successfully tested, detecting the SNP of ataxia–telangiectasia-mutated gene from both synthetic DNA and genomic DNA of *Landrace* sows. This bead-based SNP detection only required a minimal reagent amount and simplified the sample preparation procedures, thereby preserving it as a flexible and accurate detection scheme. All these characteristics show great promise in this bead-based SNP detection.

P.-C. Kao · K.-C. Li · Y.-W. Lu (✉)
Department of Bio-Industrial Mechatronics Engineering, National Taiwan University, Taipei, Taiwan, Repubic of China
e-mail: yenwenlu@ntu.edu.tw

S.-T. Ding · E.-C. Lin
Department of Animal Science, National Taiwan University, Taipei, Taiwan, Republic of China

L. Wang
Department of Electrical Engineering, National Taiwan University, Taipei, Taiwan, Republic of China

1 Introduction

Although single nucleotide polymorphisms (SNPs) appear as tiny differences between individual genome, they are perhaps one of the most important DNA sequence variations for human, crops, animals, and other species (Syvanen 2001). SNPs can be significant biomarkers, linking nucleotide sequence variations to phenotypic changes and helping researchers understand human diseases on a molecular basis (Wang and Moult 2001; Ramensky et al. 2002). To date, a great deal of work has been devoted to developing accurate, rapid, and cost-effective technologies for SNP genotyping (Kim and Misra 2007). These genotyping procedures typically involve the amplification of allele-specific products for the SNP of interest, followed by the detection techniques, such as enzymatic ligation (Landegren et al. 1988; Tong et al. 2001), enzymatic cleavage (Botstein et al. 1980; Lyamichev et al. 1999), primer extension (Sokolov 1990; Takatsu et al. 2004), split DNA enzymes G-quadruplex (Kolpashchikov 2008; Neo et al. 2011), sequencing (Li et al. 2002; Ronaghi et al. 1998), and mass spectroscopy (Tost and Gut 2005). The detection techniques utilize enzymes, molecular beacon, or fluorescent dyes to label the DNA probes, leading to the requirement of high reagent cost or complex procedures. On the other hand, using the unique property of DNA sequences in melting temperatures for SNP detection has drawn great attention since it eliminates the complex and expensive modification procedures of enzymes or

fluorescent molecules while providing a quick and accurate result (Howell et al. 1999; Russom et al. 2006; Jobs et al. 2003; Sundberg et al. 2007). Quantitative polymerase chain reaction (qPCR) and high-resolution melt (HRM) were perhaps two of the most widely used techniques, which utilized the DNA melting temperatures for SNP discrimination (Tong and Giffard 2012). A miniaturized version of this SNP detection can further reduce the reagent consumption and allow for portability of the assay in point-of-care testing.

In general, constructing miniaturized devices for SNP detection can bring many advantages over their analogues at the macroscale (Horejsh et al. 2005; Ng and Liu 2006); however, it has to address one inherent challenge in microfluidics of efficient mixing to promote the reactions. Micrometer-sized particles or beads, functioning as mobile supports, can be utilized in microfluidic systems to address such challenge and to enhance the reaction kinetics (Lim and Zhang 2007; Sochol et al. 2011). Due to their mobility, these microbeads permit better flow dynamics and mixing efficiency while preserving a high surface-to-volume ratio (Apple et al. 1999). The microbeads can also introduce additional functionalities to a microfluidic device by bearing unique surface modifications. Moreover, they reduce background noise and enhance detection sensitivity (Sochol et al. 2011). Consequently, the utilization of microbeads on microfluidic chips can significantly simplify the preparation procedures and has been an area of increasing interest. For instance, DNA sequencing and pathogenic detection have been successfully demonstrated using bead-based PCR (Hilton et al. 2012; Shendure et al. 2005; Dressman et al. 2003).

Herein, a bead-based SNP genotyping system was developed by conducting melting curve analysis for the DNA samples conjugated onto polystyrene microbeads on a microfluidic chip. One of the primary advantages in using this bead-based genotyping technique was that it was relatively easier to identify an individual microbead than it was on a planar surface when these microbeads could be properly arranged without overlapping so as not to interfere with fluorescent signals from different beads (or DNA samples). Moreover, our approach focused on altering the local temperature around the microbeads, which leads to better measurement accuracy.

Meanwhile, to simplify the SNP detection procedures, a short sequence spanning the SNP position for the melting curve analysis was adapted and was known as the dynamic allele-specific hybridization (DASH) technique (Howell et al. 1999). As a result, our bead-based SNP detection not only preserved the simple, flexible, and accurate detection scheme from DASH technique, but it also possessed the advantage of having a minimal amount of the reagents with the potential of being integrated as a lab-on-a-chip device. The microbeads with the target DNA immobilized on the surfaces were flowed in the microchannels and then hydrodynamically confined by designed fluidic traps, thereby allowing the melting curve analysis to be conducted. Both synthetic DNA and genomic DNA from *Landrace* sows on an SNP—ataxia–telangiectasia-mutated (ATM) (Lavin and Shiloh 1997; Sandoval et al. 1999) gene—were SNP genotyped and discriminated using our bead-based detection scheme. The ATM gene in *Landrace* sows was recently found to play important roles in the total number of piglets born, the number of piglets born alive, and the average birth weight of piglets due to its differential expression between the morula and blastocyst stages (Chen 2008). Our result showed this bead-based SNP detection as having great potential as an effective approach in selecting useful biomarkers and in improving the reproductive traits in sows.

2 Working principle

2.1 Melting curve analysis and dynamic allele-specific hybridization (DASH) technique

The melting temperature (T_m) of a DNA sequence is the temperature in which one half of the DNA sequence denatures and the other half is in duplex. Depending on their sequences and conformations, the DNA strands have different bonding strength, leading to their unique T_m. Based on this T_m property, the DASH technique further monitors the denaturation of a probe–target duplex in real time under homogeneous conditions using fluorescence signals. An oligonucleotide probe, specific to one allele, is hybridized to the target. This forms a duplex DNA region, which interacts with a double-stranded DNA (dsDNA)-specific intercalating dye. Upon excitation, the dye emits fluorescence proportional to the amount of dsDNA. When the sample is steadily heated, the dsDNA begins to denature with the amount of dsDNA decreasing, thereby leading to the decrease in the fluorescent intensity. When the temperature is close to the melting temperature (T_m) of the probe–target duplex, the fluorescence intensity falls rapidly. An allele-specific probe is designed to separate the melting temperatures during the analysis, which may form perfect dsDNA with wild-type single-stranded DNA (ssDNA) and one base pair mismatched with ssDNA containing SNP (allele variant).

Our study owed its simplicity and flexibility to the use of DASH methods, which were adapted with the DNA sequences conjugated on microbeads. Thus, our approach conducted the melting curve analysis at microscale, resulting in less reagent use and faster heat transfer for better temperature control, as well as being potentially

integrated with sample preparation procedures as a part of lab-on-a-chip devices.

2.2 Bead-based microfluidic device for SNP detection

Figure 1 illustrates the scheme of our proposed microbead-based SNP detection. Silica microbeads of 20 μm in diameter are coated with streptavidin and employed to bind with the biotinylated ssDNA. The DNA probe and intercalating dye are sequentially added to form the dye-intercalated probe–target conformation. Once conjugated with the target–probe duplex, the microbeads are delivered into microchannels and hydrodynamically confined by fluidic traps. The melting curve analysis is then conducted to monitor in situ the samples as the temperature increases during the DNA denaturation with the DASH technique. Due to the nucleotide mutation, one mismatch of base pair between the target–probe duplex causes a lower T_m than the perfect match one, thus detecting the SNP.

2.3 Trapping mechanism of microbead in microfluidic chips

To monitor the fluorescent signal variation and conduct the melting curve analysis, the microbeads carrying the DNA-duplex samples must be immobilized. Although a variety of microscale objects, such as cells, particles, or microbeads, were similarly immobilized in microfluidic devices for observation and assay purposes, hydrodynamic trapping was of great interest since it eliminated the need for complicated devices or external force fields (e.g., electrical or magnetic fields) to trap the cells (Tan and Takeuchi 2007; Zhang et al. 2011; Nilsson et al. 2009; Riahi et al. 2011). Using hydrodynamic forces to trap biological cells was reported (Wheeler et al. 2003; Di Carlo et al. 2006; Skelley et al. 2009). While these methods suffered from low cell-trapping efficiency, Takeuchi proposed the "self-regulating" trapping design, which employed a microfluidic channel network with the channels of different fluidic resistances to trap the cells (Tan and Takeuchi 2007) for higher trapping efficiency.

Therefore, for design simplicity, a trapping mechanism, which was adapted from Takeuchi's self-regulating trapping design and utilized different fluidic resistance to direct microbeads into an array of trap structures, was employed in this study. The trap structure was further integrated with a temperature-controlled platform to extend its functionality for the detection. Moreover, due to the introduction of the microbeads that served as a vehicle to carry the target DNA duplex, the whole microchip had the potential for possessing the capability of sample preparation and amplification via microbead manipulations in the upstream, as well as the capability of detection (e.g., SNP) in the downstream.

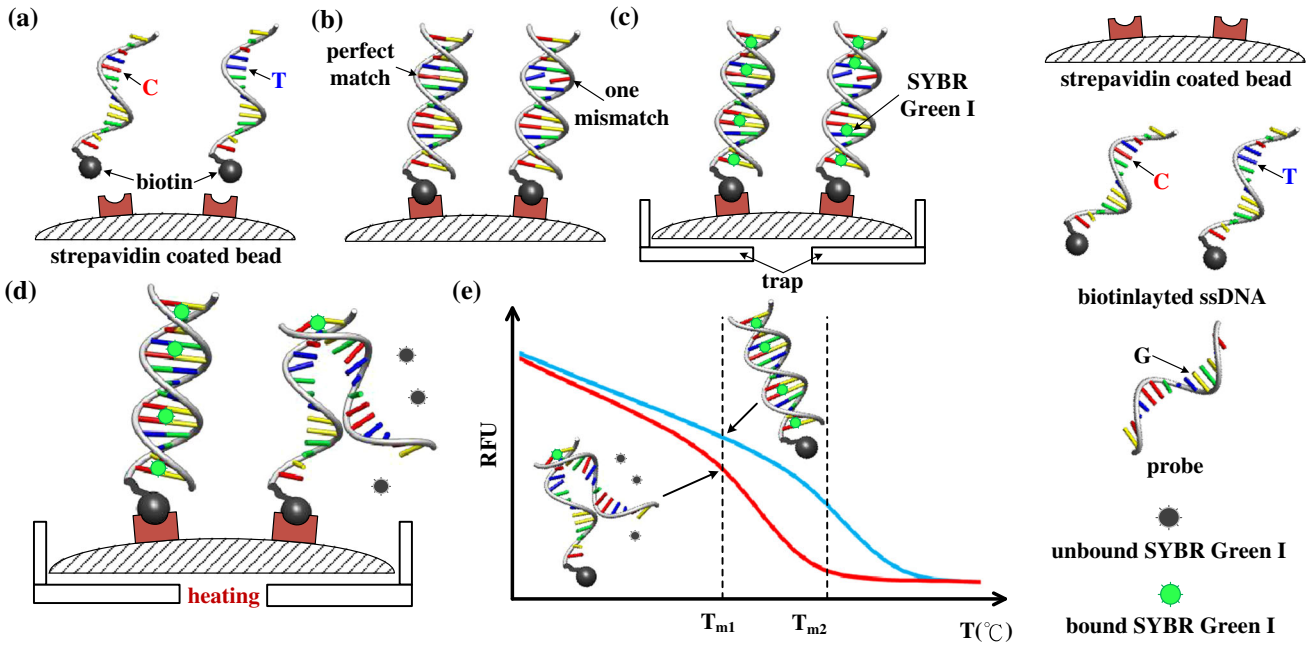

Fig. 1 Schematic workflow of the bead-based melting curve analysis technique for SNP genotyping: **a** amplification of biotinylated target ssDNA by PCR and immobilization onto streptavidin-coated bead; **b** hybridization of target ssDNA with allele-specific probe; **c** intercalation of SYBR Green I into target–probe duplex region and confinement of bead in a trap; **d** heating and monitoring and fluorescence diminishing during temperature ramping period; and **e** illustration of melting curve analysis. *Note* T_{m1}: melting temperature of normal samples (perfect match) and T_{m2}: melting temperature of mutation samples (one mismatch) (*RFU* relative fluorescence unit)

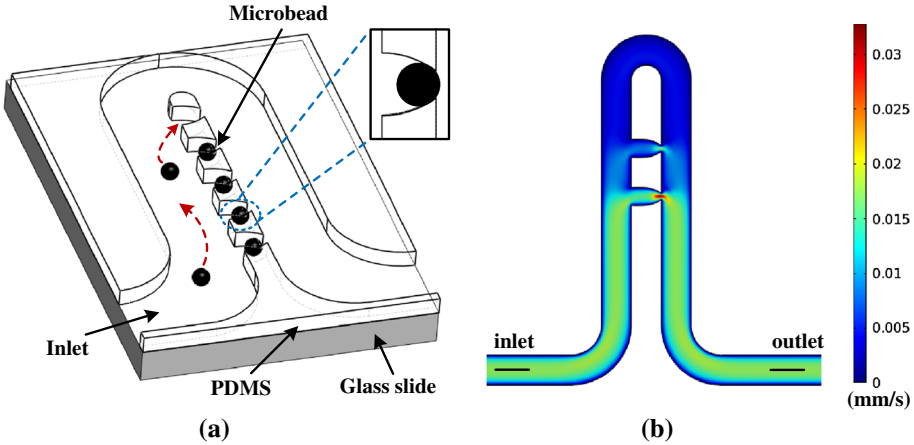

Fig. 2 Schematic illustration of bead-based microfluidic device: **a** the microbeads are injected into the microchannel and confined by the traps, which were adapted from Tan and Takeuchi (2007); **b** two-dimensional COMSOL fluid velocity field simulation of bead-based microfluidic device

Our bead-based microfluidic device consisted of the winding channels with arrays of fluidic traps, as depicted in Fig. 2 (a). When the microbeads flowed inside the microchannels, they tend to go into and stay inside the traps due to lower flow resistance. Fluid velocity field simulation was conducted using commercial finite element analysis software, COMSOL Multiphysics, version 4.0a (COMSOL, Inc., Burlington, MA, USA). The model was based on the steady-state Navier–Stokes' equation for an incompressible fluid (Sochol et al. 2011). The parameters used in the simulation were as follows: 1,000 kg/m^3 for density and 1 mPa s for dynamic viscosity (Han et al. 2010). A uniform velocity of 0.01 m/s was applied at the inlet, and a zero-pressure boundary condition was applied at the outlet. No-slip boundary conditions were set for the channel wells. As shown in the simplified two-dimensional COMSOL velocity field simulation in Fig. 2b, the flow velocity at the inlet was 0.01 mm/s and increased to more than threefold of 0.033 mm/s at the outlet of the first trap. The simulation result supported our hypothesis that the flow velocity would increase at the outlet of the traps and thereby cause a lower pressure to attract the microbeads. The differences in the flow velocity and pressure between the inlets and outlets promoted the transport of motile microbeads to these trapping locations. Moreover, once the microbeads were immobilized at the traps, the liquid flow through the occupied traps was blocked. As a result, the next vacant traps had a higher flow velocity and pressure drop, which allowed the microbeads in sequence to be hydrodynamically immobilized by an array of the traps.

3 Materials and methods

3.1 Microbead and functionalization

Plain 20-μm polystyrene microbeads (Cat. 18329-5, Polysciences Inc., Warrington, PA, USA) at 700 beads/μL were used to validate the trapping efficiency of our microfluidic devices. During the SNP detection, DNA immobilization on microbeads was achieved by using biotin–streptavidin binding as a simple and effective means. Thus, streptavidin-coated, 20-μm-diameter silica microbeads (Cat. 141048-05, Corpuscular Inc., Coldspring, NY, USA) at 250 beads/μL were employed to form the biological linker between the target sequence and microbeads (biotin–streptavidin).

3.2 Microfluidic device fabrication and design

The microfluidic device was fabricated via standard soft lithography process. Negative photoresist of SU-8 2025 (MicroChem, Newton, MA, USA) was spin-coated onto 4″ silicon wafer and patterned via photolithography. Silicone elastomer of polydimethylsiloxane (PDMS, from Sylgard 184, Dow Corning, Corning, NY, USA) at 10:1 ratio was poured upon the SU-8 mold and cured at 150 °C. After the curing process, individual microfluidic device was first punched with biopsy punch (Kai medical, Seki City, Oyana, Japan) to define the inlet and outlet of the microchannels. PDMS half-curing method was utilized to covalently bond the devices (Eddings et al. 2008). Briefly, PDMS was spin-coated on a well-cleaned 75 cm × 25 cm microscope slide and partially cured at 60 °C for 30 min to form an adhesive layer with a height of 20 μm. The PDMS sheet with microchannel patterns was then placed on the adhesive layer and cured at 150 °C for 15 min to complete the fabrication processes of bead-based microfluidic device. In addition, since the streptavidin-coated silica microbeads used in this study were 20 μm in diameter, the height and width of the microchannel were designed at 30 and 80 μm to take the poly-dispersity of the microbeads into account.

3.3 Temperature-controlled platform

A platform was developed to control the temperature of the microchannels for the melting curve analysis. A

20 mm × 32 mm of thin-film polyimide heaters (Taiwan KLC, Taichung, Taiwan) was utilized to provide a uniform and stable heating source (maximum power of 5.94 watt at 150 °C). A k-type negative temperature coefficient thermocouple (15.25 Ω at 25 °C) was mounted on the backside of the microfluidic substrate to monitor the temperature. Data acquisition system (USB6210, National Instruments) and LabVIEW (National Instruments, Austin, Texas, USA) were used to acquire the resistance variance of the thermal couple as well as to feedback control the heater. The performance of this temperature-controlled platform was calibrated and verified with the Infrared camera TVS-500EX (NEC, Tokyo, Japan). Additionally, micro-IR images were obtained to realize the temperature variations for the beads in the trapping arrays. The temperature only varied slightly with a standard deviation under 0.14 °C at 60 °C and 0.15 °C at 80 °C around the trapping array region. In other words, these microbeads in the trapping arrays experienced very similar temperature with minimal variations.

3.4 DNA extraction, amplification, and SNP discovery

The SNP discrimination point ATM-A protein gene (Basic Local Alignment Search Tool: AY587061.1)—which had been proven to be a possible biomarker associated with reproductive performance in *Landrace* sows—was chosen to demonstrate the validity and potential of our SNP detection system. The genomic DNA for SNP discovery within the ATM gene was isolated from blood samples of three individual *Landrace* sows and obtained from the anterior vena cava using a Puregene™ DNA Purification Kit (Gentra System, Inc., MN, USA). The primer pairs for the ATM gene were designed using a porcine nucleotide database (GenBank AY587061). The translation start site of the ATM gene was present within exon 3 (Rogatcheva et al. 2007). To amplify the 5′-flanking region (upstream promoter and exon 1 to intron 2 region) sequence of the ATM gene by polymerase chain reaction (PCR), the primers listed in Table 1 were used, leading to the amplification of a 1,581-bp fragment. The purified PCR products were sequenced with these primers using an automated sequencer (ABI PRISM 3730 DNA Analyzer, Applied Biosystems, Foster City, CA, USA). The nucleotide sequences were aligned for the detection of SNPs using the program Lasergene (DNAstar, Madison, WI, USA).

3.5 PCR preparation

The PCR procedure employed here was a two-step PCR to ensure the product with adequate quantity of the ssDNA sample with high specificity. The two-step PCR included a symmetric PCR and an asymmetric PCR. The first step is the symmetric PCR process in which genomic DNA was amplified to supply dsDNA containing target SNP point (ATM-A). The asymmetric PCR process followed the symmetric one, with the products from the first PCR used as template and the biotinylated forward primers applied to amplify target ssDNA. Further, to separate the dsDNA template and the ssDNA target via agarose gel electrophoresis, primers were designed to produce different lengths of DNA sequences in each step to enhance the amplification specificity. Lengths were 91-bp and 73-mer, respectively. Meanwhile, the PCR conditions were optimized to ensure sufficient and confirmed ssDNA. These were produced after a series of tests on different concentrations of forward and reverse primers with the annealing temperature in both PCR steps. The optimized PCR conditions are as follows: 5 ng/μL of genomic DNA, 200 μM dNTP mixture, 0.5 μM of Betaine, 1 % of dimethyl sulfoxide (DMSO), and 2.5 U Tag and PC2 buffer (50 mM Tris–HCl, 16 mM ammonium sulfate, and 3.5 mM $MgCl_2$) in a total reaction volume of 50 μL for the symmetric PCR. In addition, 0.2 μM of forward and reverse primers was used for the symmetric PCR to amplify the target genome region. The condition for the symmetric PCR was 94 °C for 5 min, followed by 30 cycles of 94 °C for 20 s, 55 °C for 30 s, and 72 °C for 20 s. For the asymmetric PCR, 0.5 μM of biotinylated forward primer was used to amplify and obtain the 73-mer ssDNA containing the ATM-A SNP point. The condition for the asymmetric PCR was 94 °C for 5 min, followed by 30 cycles of 94 °C for 20 s, 52 °C for 30 s, and 72 °C for 20 s. Therefore, the product for the symmetric PCR at the first step was 91-bp dsDNA amplicons, and the product for the asymmetric PCR at the second step was 73-mer ssDNA amplicons. The primers and probe in Table 1 were purchased from Protect Technology Enterprise Co., Ltd. (Taipei, Taiwan) and used without additional purification. The ssDNA probe was perfectly

Table 1 Names and sequences of the primers and probe were used in ATM gene amplification, ATM-A gene amplification, and melting curve analysis

Name	Sequence
Primer-forward (ATM)	5′-CTCCCTCTCTACCGCGTCAACGCT-3′
Primer-reverse (ATM)	5′-CCCAGTAAGAGCATATGTTCAACAT-3′
Primer-1-forward (ATM-A)	5′-CTTACCCAATACCAGCCGGGCTA-3′
Primer-1-reverse (ATM-A)	5′-TTTTACCTGAGTCTCGTCTCTCA-3′
Primer-2-forward (ATM-A)	5′-Biotin-GGCTACGTCCGAGGG-3′
Probe-(C type)	5′-CCTGCGGCTT**G**GATCATGCTG-3′

The boldface character represents the SNP position of ATM-A

matched to the CC genotype sequence as well as to one base pair mismatched to the TT genotype sequence. This two-step PCR simplified the tedious washing steps by removing the residual reagent and nonspecific DNA sequences, thereby promoting the target ssDNA binding onto the microbeads. This allowed the DASH technique to be conducted in the later procedures.

3.6 Verification of sample's genotype

To verify the genotype of the samples used in this study, samples were previously genotyped using a commercial real-time PCR machine (MyiQ, Bio-Rad). Briefly, 10 μL of 2X SYBR Green I (Applied Biosystems, Carlsbad, CA, USA) in TBE (89 mM Tris base, 89 mM boric acid, 1 mM EDTA, pH 8) and 0.5 μL of probe (10 μM) were added to 10 μL of the product of asymmetric PCR. The melting curve analysis was then performed by holding at 94 °C for 3 min and at 55 °C for 2 min and measuring the fluorescence signal for the temperature range of 60–90 °C. The data for the melting curve analysis were then processed using Bio-Rad iQ 5 2.1 Optical System Software.

3.7 Coupling of synthetic DNA and PCR DNA to microbeads

To immobilize the synthetic DNA, the reagent included 200 nM 5′-biotinylated synthetic ssDNA (73-mer, 94.9 ng), 200 nM probe, 2X SYBR Green I in TBE, and 1 μL of streptavidin-coated microbead suspension (250 beads/μL) for a total volume of 20 μL. The mixture was then incubated at 60 °C for 30 min in a heat block (DB130-1, Firstek Ltd.) to enhance the binding efficiency of streptavidin-coated beads and biotinylated target–probe duplexes. Meanwhile, to immobilize the DNA sequences from the animal samples, the asymmetric PCR products of ssDNA (73-mer, 75–200 ng), 200–500 nM probe, 2X SYBR Green I in TBE, and 1 μL of streptavidin-coated microbead suspension (250 beads/μL) with a total volume of 20 μL were mixed and incubated at 60 °C for 30 min in the heat block.

3.8 Genotyping with melting curve analysis

Prior to injecting the DNA samples, the microchannel was washed with DI-water using the syringe pump at the flow rate of 60 μL/min. The mixing reagent was then directly injected into the microfluidic device at the flow rate of 30 μL/min. Once the microbeads were completely confined by the traps, DI-water was injected at the flow rate of 60 μL/min to remove the residual reagents and to separate aggregate microbeads. The microfluidic device was then mounted on a temperature-controlled platform and assembled under an inverted fluorescence microscope (Axio Observer.A1, Carl Zeiss MicroImaging GmbH, Göttingen, Germany). The microfluidic device was heated at 70 °C for 3 min to allow the affinity capture and prevent it from being generated during the melting curve analysis. The microfluidic device was then heated from 60 to 90 °C. The filters for excitation and emission were 425–475 and 600–660 nm according to the spectra of SYBR Green I. To avoid photo bleaching, a shutter was utilized during the temperature ramping period. Epifluorescence images were obtained with a cooled charge-coupled device (CCD) camera (Retiga R-2000, *QImaging* Corp., Burnaby, BC, Canada) in every 0.5 °C and calibrated with software Q-Capture Pro (*QImaging* Corp., Burnaby, BC, Canada).

3.9 Fluorescent signal quantification

Relative fluorescence intensity of the target–probe duplex on each 20-μm-diameter microbead from the fluorescent images was quantified using image-processing software, ImageJ (National Institute of Health, Bethesda, MA, USA). The microbeads, which showed higher initial fluorescent intensity and aggregation-free, were chosen as our candidates for DASH technique since they had more target DNA bound on the microbead surface. The fluorescence intensity was then represented using a normalization function in the following equation:

$$\text{Relative fluorescence intensity} = \frac{X_{\text{i}} - X_{\text{final}}}{X_{\text{initial}}} \quad (1)$$

where X_{i} was the fluorescent intensity of a microbead; X_{final} was the final fluorescent intensity of a microbead; and X_{initial} was the initial fluorescent intensity of a microbead. The melting curve profiles were normalized starting from 100 % and ending at 0 %. Further, for statistical significance testing on our results, the p value corresponding to two homogeneous genotypes of ATM-A (CC and TT) was calculated via unpaired Student's t test. Differences with p values <0.05 were considered statistically significant.

4 Results and discussions

4.1 Bead-based microfluidic device

Ideally, one fluidic trap containing one single microbead would be used in our detection scheme. However, when excessive microbeads were stuck inside a single trap, the microbeads could aggregate. This would have blocked the flow and would have been eventually obstructed by the microbeads. A series of geometric parameters in the width, height of microchannel, the depth of the trap, and the width of inlet/outlet of each trap, as defined in Fig. 3, were

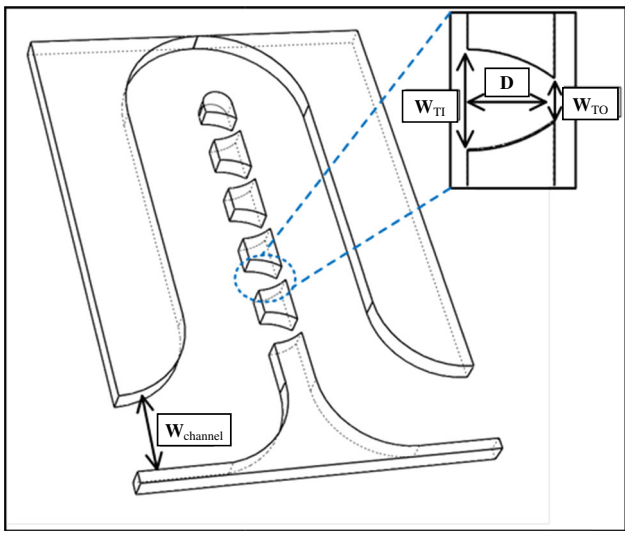

Fig. 3 Geometric parameters for a hydrodynamic trap ($W_{channel}$ width of microchannel; W_{TI} width of trap inlet; W_{TO} width of trap outlet; D depth of trap)

Table 2 Different geometrical combinations of the hydrodynamic traps to confine microbeads (diameter $D = 20$ μm) were tested in this study

Test number	$W_{channel}$ (μm)	D (μm)	W_{TI} (μm)	W_{TO} (μm)	Aggregation	Filling rate (%)
1	50	30	25	10	Yes	45
2	50	50	30	10	Yes	60
3	80	50	30	10	No	80
4	80	30	30	10	No	100

investigated to optimize the trapping efficiency of the microfluidic device. From the results listed in Table 2, the following combination with the high microbead filling ratio, or capture capability, was adapted in our device: the height and width of the microchannel in 30 and 80 μm, the depth of the trap in 30 μm, as well as the inlet and outlet for each trap in 30 and 10 μm. The bead-based microfluidic device was tested by injecting plain polystyrene microbeads of 20 μm. The experimental result in Fig. 4a validated that one fluidic trap can contain one microbead without aggregation. It also showed that after microbeads immobilized in the traps, subsequent microbead bypassed the trapping array with fully trapped microbeads. Meanwhile, a high trapping efficiency with our bead immobilization technology was confirmed.

Figure 4b confirmed that the microbeads conjugated with the target–probe duplex remained inside the fluidic traps throughout all the procedures during the melting curve analysis. Each trap contained one microbead, which permitted us to precisely conduct the melting curve analysis on individual bead. The fluorescence signal on the microbeads decayed as the temperature increased. Furthermore, the design of the hydrodynamic traps was easily integrated in a microfluidic device so the additional steps such as sample preparations and PCR amplifications could be conducted before this SNP detection, thereby having the potential of being a diagnosis platform for point-of-care applications.

4.2 SNP detection via a bead-based microfluidic device

Before conducting our SNP detection, the amplified DNA sequence of our target samples was confirmed. The PCR products of asymmetric PCR were visualized via electrophoresis on 2 % agarose gel stained with ethidium bromide and compared with the DNA marker (25/100-bp mixed DNA ladder, Bioneer). As shown in Fig. 5, the result confirmed that the dsDNA amplicons were 91 bp for the DNA template (dsDNA) and 73-mer for the biotinylated target ssDNA sequence, as expected. The light band of ssDNA, quantified by software ImageJ, is 30 % weaker than that of dsDNA. As it revealed the amount of base pairs in dsDNA, the intercalating dye of ethidium bromide only exhibited in the self-folding regions for ssDNA, leading to a relatively weaker band. To further ensure the quality of the sample, standard DNA sequencing procedures were conducted to confirm the sequence of the 73-mer single-stranded DNA amplicons with ATM-A SNP point using the commercial DNA sequencing instrument (ABI PRISM 3730 DNA analyzer).

Biotinylated ssDNA sample targets for three genotypes contained with interest position, ATM-A, were obtained after the symmetric and asymmetric PCR process. The 73-mer amplicons were verified by electrophoresis experiments. The 21-mer probes were designed complementarily with the target ssDNA specifically bounded with target DNA, and the duplex DNA was immobilized on the streptavidin microbeads. The solutions were then mixed with microbeads and reagents including SYBR Green I. The SNP genotyping analysis of each sample was performed using Rotor-Gene Q instrument and the bead-based detection scheme by monitoring the fluorescence intensity of the target–probe duplex with the temperature ranging from 65 to 85 °C. The fluorescence intensity data were then quantified and plotted.

Moreover, for the bead-based detection scheme, a number of fluorescence images from the multiple microbeads were collected and image-processed. It was found that different individual microbeads presented different intensities of the fluorescence signals at the same temperature, as illustrated in Fig. 4b, owing to the fact that different amounts of DNA conjugated with the microbeads. However, further studies showed similar tendency of the fluorescence intensity variation for each individual bead

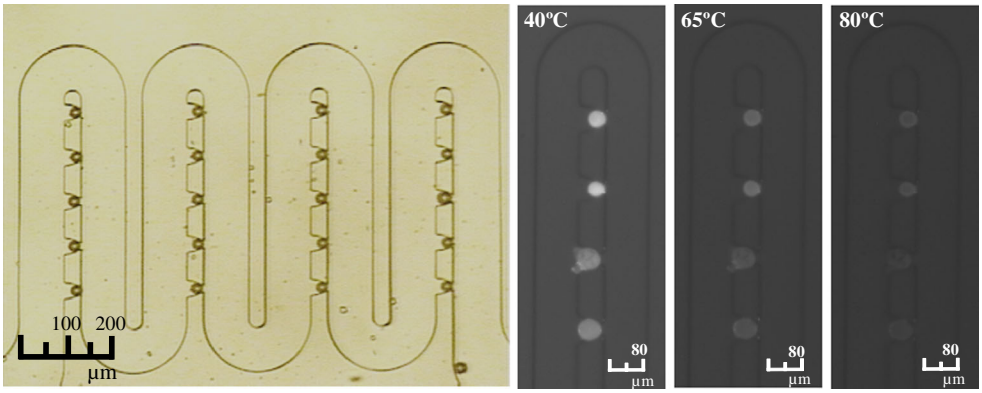

Fig. 4 **a** Micrograph from a microbead trapping experiment, showing confinement of 20-μm-diameter microbeads and **b** epifluorescence micrographs of the target–probe-duplex-conjugated microbeads at 40, 65, and 80 °C

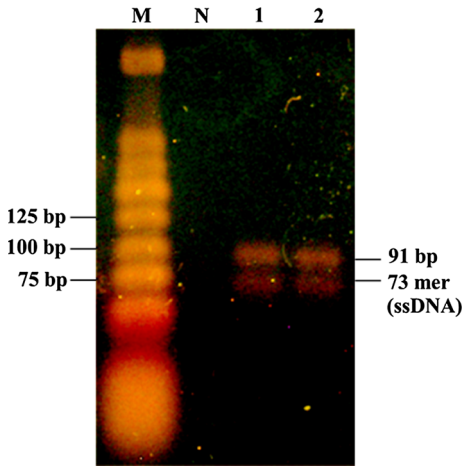

Fig. 5 A photograph of an agarose gel electrophoresis of amplified DNA of the ATM-A gene region from two *Landrace* sows run against a negative control. The results from the asymmetric PCR products verified the existence of 73-mer ssDNA amplicons (CC and TT samples). *Note M* DNA marker; *N* negative control; *1* asymmetric PCR product of perfect-match sample (CC); *2* asymmetric PCR product of one-mismatch sample (TT)

during the melting curve analysis. The microbeads with the same DNA sequence had almost same melting temperatures and melting curve behaviors. Therefore, the melting curves could be normalized and presented as the relationship between the temperature and relative fluorescent unit (RFU).

The melting curves of the synthetic target DNAs—the samples with homozygous and heterozygous genotypes—from both detection techniques were then obtained, as shown in Fig. 6. The profile of the TT sample had a higher decreasing rate than the one of the CC sample due to the larger binding forces between the probe and target ssDNA. The maximum slope change of the melting curve, or the value of the negative first derivatives of the curve, was determined as the melting temperature. The melting temperatures (T_m) for the synthetic samples with TT and CC were conservatively estimated to overlap the two peaks of the melting curve for the CT samples. The T_m values of TT and CC were, respectively, 76.0 and 79.0 °C by using Rotor-Gene Q, while they were 75.5 and 78.4 °C by using our bead-based detection scheme. The melting temperature differences (ΔT_m) for the synthetic samples with TT and CC from both techniques were comparable (3.0 and 2.9 °C). Meanwhile, the heterozygous sample (CT) showed a combinative profile of both homozygous samples (CC and TT).

To test our bead-based detection scheme on practical samples, the melting curve analysis on sow samples with three most frequent variants in one SNP location was performed by using our bead-based detection scheme and confirmed by Rotor-Gene Q instrument, as shown in Fig. 7. The melting curves on sow samples obtained by using both detection methods were similar to those on synthetic target DNA samples. The peaks of the TT samples slightly shifted from 76.0 (synthetic) to 73.5 °C (sow) by using Rotor-Gene Q, compared to the values shifted from 75.5 to 73.0 °C by using our bead-based scheme. Likewise, the peaks of the CC samples shifted to lower values. One of the major reasons for this temperature shift was because the synthetic DNA samples showed higher melting temperature values due to additional DNA fragments and biomolecules in the genomic DNA samples. In addition, the heating rate during the melting process could affect the melting temperature. As the heating rates increased, the melting process deviated from the equilibrium, so the melting temperature also shifted to higher values (Russom et al. 2006; Gundry et al. 2003; Hannewijk and Haighton 1958). Our bead-based prototypes currently had a heating rate of 2 °C/min, compared to a heating rate of 3 °C/min from the commercial Rotor-Gene Q instrument, leading to

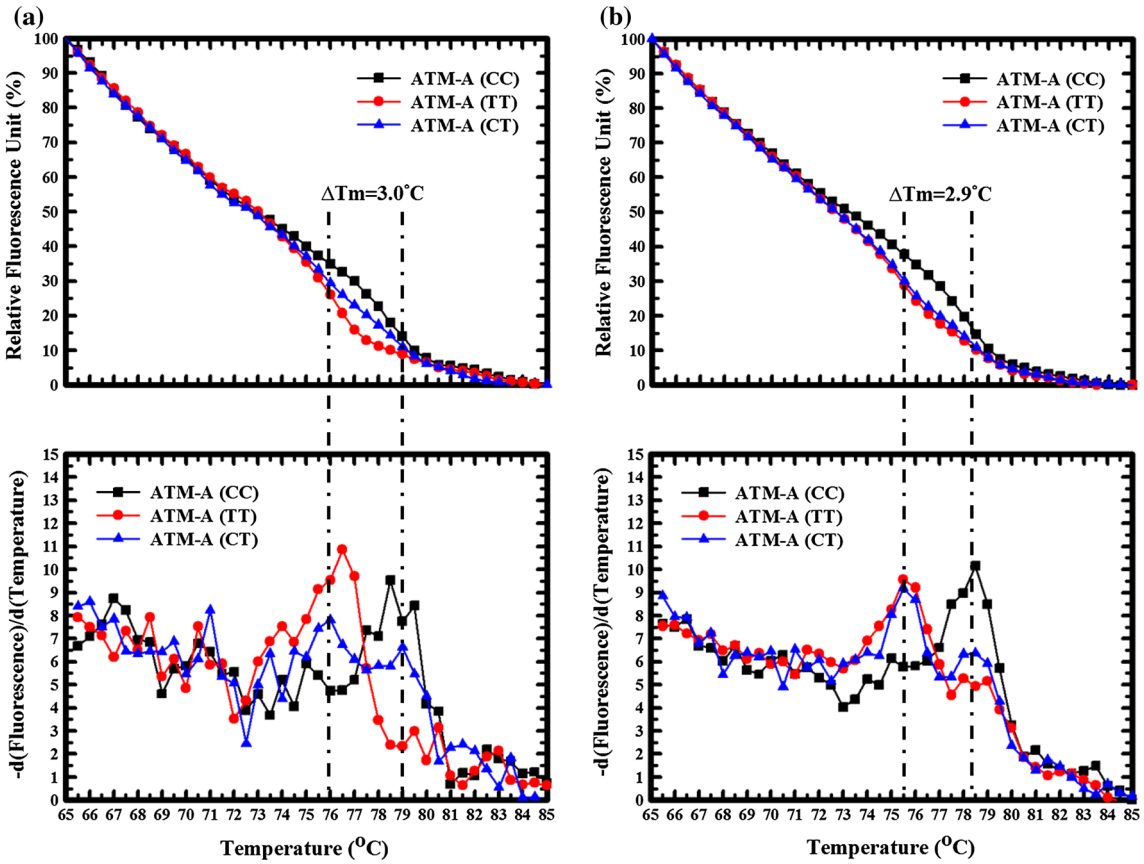

Fig. 6 Melting curves and the negative first derivatives (−dF/dT) for three types of synthetic DNA samples of the ATM-A polymorphism (CC, TT, and CT) using **a** the Rotor-Gene Q qPCR instrument and **b** the bead-based microfluidic device. The melting temperature differences of qPCR machine and our device were 3 and 2.9 °C between CC and TT genotypes. *Note* The melting temperatures (T_m) for the samples with TT and CC were conservatively estimated to overlap the two peaks of the melting curve from the CT sample

lower melting temperatures and slightly smaller temperature differences ($\Delta T_m = 2.5$ °C for Rotor-Gene Q system; $\Delta T_m = 1.5$ °C for bead-based detection prototype). However, compared to the rigorous specificity of the thermocycler in Rotor-Gene Q system, this prototype gave similar levels of discrimination on the results and enabled unambiguous allele scoring using our bead-based detection.

The reliability of our SNP detection scheme was also examined. Figure 8 summarized our results from at least four microbeads on different allele variants. The average value of the melting temperature from three independent experiments in the CC genotype sample FC-363 was 75 ± 0.71 °C, with the average value of the melting temperature for the TT genotype sample FC-636 being 72.63 ± 0.25 °C. The p value was 3×10^{-4}, proving that the perfect-match sample (CC) could be statistically distinguished from the one-mismatch sample (TT).

However, there were a few issues to be considered while this bead-based melting curve analysis was applied. Firstly, the technique was limited by the sequence length in two aspects: (1) the probe length and (2) the sequence length of the DNA amplicons used for the melting curve analysis. Generally, 15–21 nucleotides in the probe length are recommended for conventional tube-based melting curve analysis (Howell et al. 1999). Meanwhile, the sequence length of the DNA amplicons used for the melting curve analysis affected the melting temperature: the longer the DNA amplicons, the higher the T_m is. For instance, DNA amplicons from 167 (Lipsky et al. 2001) to 212 bp (Elenitoba-Johnson and Bohling 2001) were tested by melting curve analysis with SYBR Green I. Longer sequences (up to 1,000 bp) of DNA amplicons were also demonstrated when LCGreen® (one of saturating double-stranded-nucleic-acid-specific fluorescent dyes) was used as the intercalated dyes (Montgomery et al. 2007). These design considerations in the sequence length were taken for conventional melting curve analysis in tube-based configurations. The bead-based version of the technique thus needed more study to gain the related knowledge and to know its limitation, as the microbeads could provide better flow dynamics and mixing efficiency for the DNA samples.

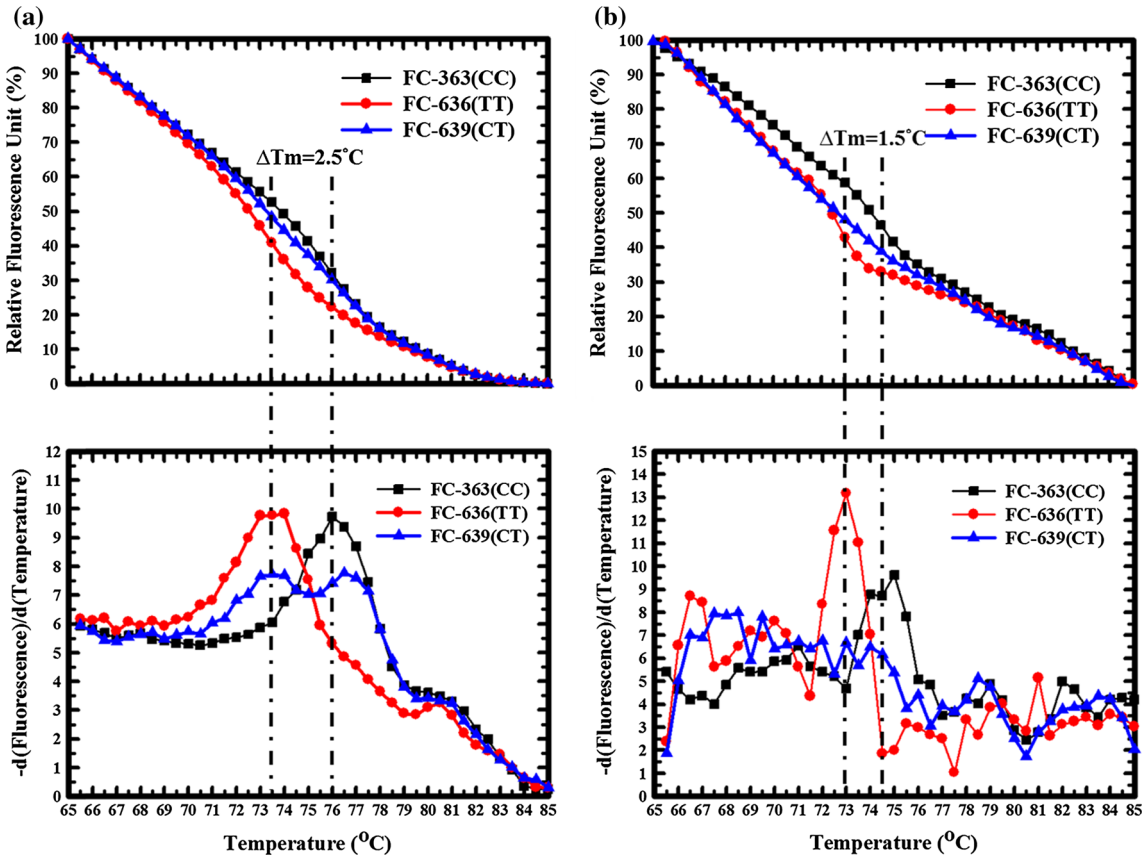

Fig. 7 Melting curves and the negative first derivatives (−dF/dT) for three sow samples using **a** the Rotor-Gene Q qPCR instrument and **b** the developed bead-based microfluidic device. *Each graph* shows three variant curves according to the polymorphism (CC, TT, and CT). The melting temperature differences of the qPCR machine and our device were 2.5 and 1.5 °C between CC and TT genotypes. The assayed genomic DNAs were known genotypes as follows: Two homozygous genotypes were processed as the perfect-match duplex (*filled square*) and one-mismatch duplex (*filled circle*) with the probe; heterozygotes were represented as (*filled triangle*). *Note* The melting temperatures (T_m) for the samples with TT and CC were conservatively estimated to overlap the two peaks of the melting curve from the CT sample. *Note II* FC-363, FC-636, and FC-639 represented different sow identification numbers in the farm. Each sow had different allele types

Secondly, although the two-step PCR adapted here could have produced specific ssDNA amplicons (which was convenient during our initial development of the technology to prove the concept), it required simplification for the development of an integrated sample-to-answer system. While the one-step asymmetric PCR could have been applied to the SNP detection, the experimental parameters (e.g., primer design, PCR cycles, PCR annealing temperature, and the ratio between two primers for high specificity) needed to be optimized. Therefore, efforts to adapt the one-step asymmetric PCR in our experiment had to be made.

Finally, our bead-based SNP detection showed the consistent and accurate discrimination capability, thereby distinguishing a single nucleotide difference from that of a DNA sequence. It also possessed unique merits in various aspects. First, it served as one of the key modules during diagnosis, which allowed easy integration into a microfluidic device for performing a series of sample preconditioning. Next, the bead-based detection only required a small number of microbeads, whose diameter had the potential of being smaller than the ones used in this study (i.e., diameter $D = 20$ μm). Therefore, the DNA amplicons used for the detection on the microbeads could be consumed much less than the traditional tube-based SNP technique. Such reduction on sample consumption would be very beneficial for applications on low-volume clinical samples. Furthermore, the microbeads allowed the DNA test sample to be concentrated on the surface of the microbeads. This would confine the fluorescent signals around the microbeads and enhance the signal-to-background ratio for better detection as compared to traditional tube-based SNP technique.

While our prototypes only showed three genotypes in liquid flows, the detection scheme could be further extended to increase parallelization by delivering microbeads to

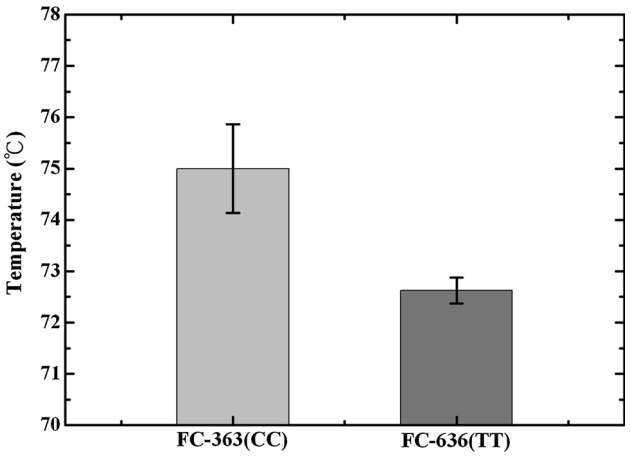

Fig. 8 Melting temperature for the samples of FC-363 ($n = 4$) and FC-636 ($n = 4$) ($p = 3 \times 10^{-4}$)

an array of microchannels, with each microchannel being responsible for distinct reactions or samples. As such, multiplexing capability could be obtained by immobilizing individual bead prior to melting curve analysis and encoding the beads with different fluorescent dyes. The microbeads in a variety of sizes and shapes could be employed to further promote the multiplexing.

5 Conclusions

A novel SNP genotyping scheme, which performed the melting curve analysis technique on the DNA duplexes on microbeads in microfluidic devices, was successfully demonstrated. Its genotyping results for the DNA sequences from synthetic genes and sow samples from the farm were evaluated, with results comparable to those obtained from traditional tube-based instruments. This thereby verified the reliability of our proposed scheme. The microbeads provided a relatively high surface-to-volume ratio for biomolecule immobilization, which has the potential of enhancing reaction kinetics and improving the sensitivity. This scheme also required minimal reagent amount and employed simple sample preparations, compared to tube-based approaches, while preserving it as a flexible, rapid, and accurate SNP detection. Although the two-step PCR procedure employed here could be complex, the DNA sample preparation was being simplified into a one-step PCR procedure, which would be convenient for system integration and lab-on-a-chip development. All the above showed this bead-based SNP detection on a microchip to have great potential as a cost-effective SNP detection method to support genotyping applications.

Acknowledgments The authors thank Dr. L. C. Chen and Mr. J. H. Weng in Department of Bio-Industrial Mechatronics Engineering (BIME) at National Taiwan University (NTU) for the assistance in qPCR technique, and the Center of Biotechnology at NTU for providing samples and SNP genotyping technique. The authors also thank Dr. J. C. Hsu in Department of Entomology at NTU for professional guidance in SNP genotyping techniques, as well as Mr. C.-M. Lin and Ms. T. Kirk for manuscript editing. This project was supported by the Center of Biotechnology at NTU and National Science Council, Taiwan (NSC 102-2221-E-002-084-MY3).

References

Apple FS, Christenson RH, Valdes R, Andriak AJ, Berg A, Duh SH, Feng YJ, Jortani SA, Johnson NA, Koplen B, Mascotti K, Wu AHB (1999) Simultaneous rapid measurement of whole blood myoglobin, creatine kinase MB, and cardiac troponin I by the triage cardiac panel for detection of myocardial infarction. Clin Chem 45:199–205

Botstein D, White RL, Skolnick M, Davis RW (1980) Construction of a genetic-linkage map in man using restriction fragment length polymorphisms. Am J Hum Genet 32:314–331

Chen Y-H (2008) The identification of litter size related single nucleotide polymorphisms from differentially regulated genes of early embryo in Landrace sows. Master dissertation, National Taiwan University

Di Carlo D, Aghdam N, Lee LP (2006) Single-cell enzyme concentrations, kinetics, and inhibition analysis using high-density hydrodynamic cell isolation arrays. Anal Chem 78:4925–4930

Dressman D, Yan H, Traverso G, Kinzler KW, Vogelstein B (2003) Transforming single DNA molecules into fluorescent magnetic particles for detection and enumeration of genetic variations. Proc Natl Acad Sci 100:8817–8822

Eddings MA, Johnson MA, Gale BK (2008) Determining the optimal PDMS–PDMS bonding technique for microfluidic devices. J Micromech Microeng 18:067001

Elenitoba-Johnson KSJ, Bohling SD (2001) Solution-based scanning for single-base alterations using a double-stranded DNA binding dye and fluorescence-melting profiles. Am J Pathol 159:845–853

Gundry CN, Vandersteen JG, Reed GH, Pryor RJ, Chen J, Wittwer CT (2003) Amplicon melting analysis with labeled primers: a closed-tube method for differentiating homozygotes and heterozygotes. Clin Chem 49:396–406

Han C, Zhang Q, Ma R, Xie L, Qiu T, Wang L, Mitchelson K, Wang J, Huang G, Qiao J, Cheng J (2010) Integration of single oocyte trapping, in vitro fertilization and embryo culture in a microwell-structured microfluidic device. Lab Chip 10:2848–2854

Hannewijk J, Haighton AJ (1958) Differential thermal analysis. 3. Melting curves of oils and fats. J Am Oil Chem Soc 35:457–461

Hilton J, Nguyen T, Barbu M, Pei R, Stojanovic M, Lin Q (2012) Bead-based polymerase chain reaction on a microchip. Microfluid Nanofluid 13:749–760

Horejsh D, Martini F, Poccia F, Ippolito G, Di Caro A, Capobianchi MR (2005) A molecular beacon, bead-based assay for the detection of nucleic acids by flow cytometry. Nucleic Acids Res 33:e13

Howell WM, Jobs M, Gyllensten U, Brookes AJ (1999) Dynamic allele-specific hybridization. A new method for scoring single nucleotide polymorphisms. Nat Biotechnol 17:87–88

Jobs M, Howell WM, Stromqvist L, Mayr T, Brookes AJ (2003) DASH-2: flexible, low-cost, and high-throughput SNP genotyping by dynamic allele-specific hybridization on membrane arrays. Genome Res 13:916–924

Kim S, Misra A (2007) SNP genotyping: technologies and biomedical applications. Annu Rev Biomed Eng 9:289–320

Kolpashchikov DM (2008) Split DNA enzyme for visual single nucleotide polymorphism typing. J Am Chem Soc 130:2934–2935

Landegren U, Kaiser R, Sanders J, Hood L (1988) A ligase-mediated gene detection technique. Science 241:1077–1080

Lavin MF, Shiloh Y (1997) The genetic defect in ataxia-telangiectasia. Annu Rev Immunol 15:177–202

Li Q, Liu Z, Monroe H, Culiat CT (2002) Integrated platform for detection of DNA sequence variants using capillary array electrophoresis. Electrophoresis 23:1499–1511

Lim CT, Zhang Y (2007) Bead-based microfluidic immunoassays: the next generation. Biosens Bioelectron 22:1197–1204

Lipsky RH, Mazzanti CM, Rudolph JG, Xu K, Vyas G, Bozak D, Radel MQ, Goldman D (2001) DNA melting analysis for detection of single nucleotide polymorphisms. Clin Chem 47:635–644

Lyamichev V, Mast AL, Hall JG, Prudent JR, Kaiser MW, Takova T, Kwiatkowski RW, Sander TJ, de Arruda M, Arco DA, Neri BP, Brow MAD (1999) Polymorphism identification and quantitative detection of genomic DNA by invasive cleavage of oligonucleotide probes. Nat Biotechnol 17:292–296

Montgomery J, Wittwer CT, Palais R, Zhou LM (2007) Simultaneous mutation scanning and genotyping by high-resolution DNA melting analysis. Nat Protoc 2:59–66

Neo JL, Aw KD, Uttamchandani M (2011) Visual SNP genotyping using asymmetric PCR and split DNA enzymes. Analyst 136:1569–1572

Ng J, Liu W-T (2006) Miniaturized platforms for the detection of single-nucleotide polymorphisms. Anal Bioanal Chem 386:427–434

Nilsson J, Evander M, Hammarstrom B, Laurell T (2009) Review of cell and particle trapping in microfluidic systems. Anal Chim Acta 649:141–157

Ramensky V, Bork P, Sunyaev S (2002) Human non-synonymous SNPs: server and survey. Nucleic Acids Res 30:3894–3900

Riahi R, Mach KE, Mohan R, Liao JC, Wong PK (2011) Molecular detection of bacterial pathogens using microparticle enhanced double-stranded DNA probes. Anal Chem 83:6349–6354

Rogatcheva MB, Fritz KL, Rund LA, Pollock CB, Beever JE, Counter CM, Schook LB (2007) Characterization of the porcine ATM gene: towards the generation of a novel non-murine animal model for ataxia-telangiectasia. Gene 405:27–35

Ronaghi M, Uhlen M, Nyren P (1998) A sequencing method based on real-time pyrophosphate. Science 281:363–365

Russom A, Haasl S, Brookes AJ, Andersson H, Stemme G (2006) Rapid melting curve analysis on monolayered beads for high-throughput genotyping of single-nucleotide polymorphisms. Anal Chem 78:2220–2225

Sandoval N, Platzer M, Rosenthal A, Dörk T, Bendix R, Skawran B, Stuhrmann M, Wegner R-D, Sperling K, Banin S, Shiloh Y, Baumer A, Bernthaler U, Sennefelder H, Brohm M, Weber BHF, Schindler D (1999) Characterization of ATM gene mutations in 66 ataxia telangiectasia families. Hum Mol Genet 8:69–79

Shendure J, Porreca GJ, Reppas NB, Lin X, McCutcheon JP, Rosenbaum AM, Wang MD, Zhang K, Mitra RD, Church GM (2005) Accurate multiplex polony sequencing of an evolved bacterial genome. Science 309:1728–1732

Skelley AM, Kirak O, Suh H, Jaenisch R, Voldman J (2009) Microfluidic control of cell pairing and fusion. Nat Methods 6:147–152

Sochol RD, Casavant BP, Dueck ME, Lee LP, Lin L (2011) A dynamic bead-based microarray for parallel DNA detection. J Micromech Microeng 21:054019

Sokolov BP (1990) Primer extension technique for the detection of single nucleotide in genomic DNA. Nucleic Acids Res 18:3671

Sundberg SO, Wittwer CT, Greer J, Pryor RJ, Elenitoba-Johnson O, Gale BK (2007) Solution-phase DNA mutation scanning and SNP genotyping by nanoliter melting analysis. Biomed Microdevices 9:159–166

Syvanen A-C (2001) Accessing genetic variation: genotyping single nucleotide polymorphisms. Nat Rev Genet 2:930–942

Takatsu K, Yokomaku T, Kurata S, Kanagawa T (2004) A FRET-based analysis of SNPs without fluorescent probes. Nucleic Acids Res 32:e156

Tan W-H, Takeuchi S (2007) A trap-and-release integrated microfluidic system for dynamic microarray applications. Proc Natl Acad Sci 104:1146–1151

Tong SYC, Giffard PM (2012) Microbiological applications of high-resolution melting analysis. J Clin Microbiol 50:3418–3421

Tong AK, Li Z, Jones GS, Russo JJ, Ju J (2001) Combinatorial fluorescence energy transfer tags for multiplex biological assays. Nat Biotechnol 19:756–759

Tost J, Gut IG (2005) Genotyping single nucleotide polymorphisms by MALDI mass spectrometry in clinical applications. Clin Biochem 38:335–350

Wang Z, Moult J (2001) SNPs, protein structure, and disease. Hum Mutat 17:263–270

Wheeler AR, Throndset WR, Whelan RJ, Leach AM, Zare RN, Liao YH, Farrell K, Manger ID, Daridon A (2003) Microfluidic device for single-cell analysis. Anal Chem 75:3581–3586

Zhang Y, Park S, Liu K, Tsuan J, Yang S, Wang T-H (2011) A surface topography assisted droplet manipulation platform for biomarker detection and pathogen identification. Lab Chip 11:398–406